SCIENCE CHINA
Information Sciences

• **Supplementary File** •

Pyramid-resolution Person Restoration for Cross-Resolution Person Re-identification

Chunlei PENG[1,2], Bo WANG[1,2], Decheng LIU[1,2], Nannan WANG[1,3*] & Xinbo GAO[4]

[1]*State Key Laboratory of Integrated Services Networks, Xidian University, Shaanxi* 710071*, China;*
[2]*School of Cyber Engineering, Xidian University, Shaanxi* 710071*, China;*
[3]*School of Telecommunications Engineering, Xidian University, Shaanxi* 710071*, China;*
[4]*Chongqing Key Laboratory of Image Cognition, Chongqing University of Posts and Telecommunications, Chongqing* 400065*, China*

Appendix A Inspiration

Traditional person re-identification (ReID) methods typically rely on the assumption that both gallery and query images have high resolutions. However, in real-world scenarios, this assumption often doesn't hold due to the influence of camera technology and the distances between cameras and target individuals. To solve this problem, cross-resolution person ReID [1–7] has been noticed in recent years. Metric learning and dictionary pair learning [8] were utilized in some early attempts to reduce the resolution gap. In addition, some researchers [4,9] have reduced the impact of resolution variation on cross-resolution ReID by learning the resolution-invariant representation. However, in unconstrained scenarios, it is difficult for these methods to learn a feature that is robust to person images with various resolutions. Subsequently, with the development of super-resolution (SR), some researchers tried to introduce SR techniques to cross-resolution person ReID tasks. Although these methods [7, 10] have shown some performance improvements in cross-resolution person ReID, they can only obtain an image with a fixed ratio to the original image size, which is difficult to adapt to more complex scenarios. To address this problem, some researchers [3, 11] have used multiple fixed ratio image restoration models to deal with more complex person ReID scenarios. Pyramid strategy has been utilized in person re-identification before. [31] applied pyramid pooling to extract spatial pyramid features, which used the error from robust reconstruction over spatial pyramid features to measure similarities between two persons. However, it intended to cope with occlusion problem in traditional person ReID, and the pyramid features were extracted from parts of the person images. [32] proposed an attention pyramid method for person ReID, which exploited the attention regions in a pyramid way. [33] extracted features from different layers of the networks and aggregated them in a pyramid structure for person ReID. However, these existing methods applied the pyramid strategy of part image, attention region, or layer features in traditional person ReID task, while pyramid resolution restoration for cross-resolution person ReID has not been explored before. In fact, the usage of pyramid resolution restoration is reasonable in cross-resolution scenario, but it is difficult to set proper fixed pyramid resolutions for restoration, especially when dealing with real-world person ReID conditions with irregular aspect ratios and resolutions of gallery images and query images. Fig. A1 shows example pairs of traditional ReID, cross-resolution ReID and multi-resolution ReID for unconstrained scenarios. It is evident that learning only the resolution-invariant representation of the image or restoring the image by predefining the target resolution is not sufficient. This is because it is difficult to specify an appropriate resolution for restoration in multi-resolution scenarios, and it is difficult to learn robust resolution-invariant features.

To overcome these challenges, we propose a pyramid-resolution person restoration method for cross-resolution person ReID. High quality images with pyramid resolution are obtained by restoring the original images with our method, and the valid information from the pyramid resolution images are fully mined by the person ReID models with different parameters. We design a parallel pyramid reconstruction structure that can be easily combined with classical image restoration models. By combining with a classical image restoration feature extractor, we are able to obtain multiple images with pyramid resolution, thus reducing the impact of multi-resolution images on person ReID. Extensive experiments are conducted on the multi-resolution real-world dataset MTA-ReID [12], as well as widely used cross-resolution simulated ReID datasets including MLR-DukeMTMC [1, 13], MLR-Market1501 [1, 14], and MLR-CUHK03 [1, 15], which have demonstrated the effectiveness and superiority of our proposed method.

Appendix B Pyramid-resolution Restoration Network

After obtaining the feature, high-quality images with pyramid-resolution are obtained by the pyramid-resolution image reconstructor we have designed. The pyramid-resolution reconstructor consists of three branches, each corresponding to a different resolution image. Inspired by [16], each branch employs a 3×3 convolution layer and a Leaky ReLU layer to transform the extracted original image feature before upsampling the feature. This is to allow the features extracted by different feature extractors to be adapted to the consequent upsampling process. In upsampling, the number of channels of the feature is first boosted by a convolution layer, and then the corresponding upsampling is performed using PixelShuffle [17]. The main task of PixelShuffle is to take a low-resolution feature map and reconstruct it by convolution and multichannel reorganization to obtain a high-resolution feature map. Finally, a convolution layer is used to convert the upsampled feature into the final output RGB image. The specific channel number variations and the height and width variations are shown in Table B1.

In the pyramid-resolution restoration network, in order to make our restored images more realistic, we optimise the whole network by minimising the mean absolute error (MAE) loss. The specific formula is as follows:

$$L_{h1} = \| X_{h1} - R_1(X_h) \|, \tag{B1}$$

* Corresponding author (email: nnwang@xidian.edu.cn)

a) Traditional ReID b) Cross-resolution ReID c) Multi-resolution ReID

Figure A1 Person ReID situations where examples of query-gallery pairs are presented. a) Traditional ReID examples from Market1501 with same resolution pairs. b) Cross-resolution ReID examples from MLR-Market1501 with cross-resolution pairs. c) Multi-resolution ReID examples from MTA-ReID with various resolution.

Table B1 Architecture of the Pyramid-resolution Images Reconstructor

Branch	Stage	Network	Output
1	before upsample	Conv 3×3	W×H, 64
		Leaky ReLU	W×H, 64
	upsample	Conv 3×3	W×H, 256
		PixShuffle(2)	2W×2H, 64
		Conv 3×3	2W×2H, 256
		PixShuffle(2)	4W×4H, 64
	after upsample	Conv 3×3	4W×4H, 3
2	before upsample	Conv 3×3	W×H, 64
		Leaky ReLU	W×H, 64
	upsample	Conv 3×3	W×H, 576
		PixShuffle(3)	3W×3H, 64
	after upsample	Conv 3×3	3W×3H, 3
3	before upsample	Conv 3×3	W×H, 64
		Leaky ReLU	W×H, 64
	upsample	Conv 3×3	W×H, 256
		PixShuffle(2)	2W×2H, 64
	after upsample	Conv 3×3	2W×2H, 3

$$L_{h2} = \| X_{h2} - R_2(X_h) \|, \tag{B2}$$

$$L_{h3} = \| X_{h3} - R_3(X_h) \|, \tag{B3}$$

$$L = L_{h1} + \alpha L_{h2} + \beta L_{h3}, \tag{B4}$$

where $R_i(X_h)$ is responsible for resizing X_h to the size of its corresponding image through bicubic interpolation, and α, β are hyperparameters used to control the importance of the MAE loss for different branches. It should be noticed that bicubic interpolation can also be regarded as one kind of image restoration technique, which has been widely applied in traditional image processing tasks. In order to cope with unconstrained cross-resolution person ReID situations, our method intends to take advantage of deep learning based image restoration models which can generate high quality restored images. In equation (B1), (B2), (B3) here, we utilize the MAE loss between the restored images X_{h1}, X_{h2}, X_{h3} and the original input image X_h to ensure the fidelity of the restored images. The restored images by our pyramid-resolution restoration network and ablation study on replacing the network with simple bicubic interpolation are presented in Appendix C.3 below.

Appendix C Experiments

Appendix C.1 Experiments on Multi-resolution Dataset

When person ReID is in the unconstrained situation, the resolution of the captured person images are various, which can seriously affect the performance of person ReID. Table C1 compares our approach with the three state-of-the-art person ReID algorithms. On the multi-resolution dataset MTA-ReID [12], the Strong Baseline method [18] achieves 25.8%, 50.5%, 69.7%, and 74.9% on mAP, rank-1, rank-5, and rank-10, respectively, using effective training tricks. The AGW method [19] designs an Attention Generalized mean pooling with weighted triplet loss achieving 27.7%, 53.8%, 71.7%, and 76.5% on this multi-resolution dataset. The ABD method [20] achieves 30.8%, 59.7%, 74.1%, 78.2% by integrating the attention module and diversity regularization. The OSNet

Table C1 Experimental results (%) on multi-resolution MTA-ReID dataset.

Method	backbone	mAP	Rank-1	Rank-5	Rank-10
Strong Baseline [18]	ResNet50	25.8	50.5	69.7	74.9
AGW [19]		27.7	53.8	71.7	76.5
ABD [20]		30.5	56.6	72.4	76.8
OSNet [21]	OSNet	30.8	59.7	74.1	78.2
Ours (SwinIR)		**34.4**	**63.0**	**75.8**	**79.8**
Ours (HAN)		**34.9**	**63.0**	**75.9**	**80.0**

Table C2 Experimental results (%) on cross-resolution datasets.

Method	backbone	MLR-CUHK03				MLR-Market1501				MLR-DukeMTMC			
		mAP	Rank-1	Rank-5	Rank-10	mAP	Rank-1	Rank-5	Rank-10	mAP	Rank-1	Rank-5	Rank-10
JUDEA [2]	-	-	26.2	58.0	73.4	-	-	-	-	-	-	-	-
SDF [22]		-	22.2	48.0	64.0	-	-	-	-	-	-	-	-
SING [1]		-	67.7	90.7	94.7	-	74.4	87.8	91.6	-	65.2	80.1	84.8
CSR-GAN [3]	VGG-19	-	71.3	92.1	97.4	58.3	76.4	88.5	91.9	-	67.6	81.4	85.1
FFSR+RIFE [9]	ResNet50	38.5	73.3	92.6	-	59.5	75.4	88.7	91.0	-	-	-	-
RAIN [29]		-	78.9	97.3	98.7	-	-	-	-		-	-	-
CAD-Net [4]		-	82.1	97.4	98.8	-	83.7	92.7	95.8	-	75.6	86.7	89.6
CAD-Net++ [27]		-	83.4	98.1	99.1	-	84.1	93.0	96.2	-	77.2	88.1	90.4
PRI [28]		-	86.5	97.7	99.1	-	88.1	94.2	96.5	-	82.1	91.1	92.8
B-F+RFD [5]		-	-	-	-	-	86.9	95.6	97.4	-	82.9	92.0	94.0
ASPR [7]		-	84.1	97.5	98.7	-	-	-	-	-	-	-	-
LRAR [23]		-	89.2	98.9	99.8	-	90.1	96.2	97.7	-	-	-	-
CRGAN [24]		-	88.4	96.9	98.2	-	88.4	95.2	96.8	-	79.6	88.6	92.0
DSCWT [26]		-	86.0	93.3	-	-	83.3	92.9	-	-	75.9	86.4	-
MRJL [30]	PCB	-	80.7	95.7	-	-	90.1	95.6	-	-	-	-	-
SR-DSFF [25]	ResNet101	-	91.8	97.5	99.2	-	90.9	96.4	97.6	-	-	-	-
PS-HRNet [11]	HRNet	-	92.6	98.3	99.4	-	91.5	96.7	97.9	-	-	-	-
INTACT [10]	OSNet	-	86.4	97.4	98.5	-	88.1	95.0	96.9	-	81.2	90.1	92.8
JBIM (OSNet) [6]		90.3	88.7	97.5	99.0	74.7	89.6	96.2	97.7	-	-	-	-
Ours (SwinIR)		**97.5**	**98.1**	**99.4**	**99.9**	**84.3**	**93.7**	**97.3**	**98.4**	**76.5**	**87.6**	**93.9**	**95.7**
Ours (HAN)		**97.8**	**98.7**	**99.7**	**100.0**	**84.8**	**93.8**	**97.4**	**98.5**	**76.7**	**87.9**	**93.7**	**95.6**

achieves 30.5%, 56.6%, 72.4%, 76.8% by learning omni-scale features of images. Our method using the HAN feature extractor achieved 34.9%, 63.0%, 75.9%, and 80.0%, respectively, which are much higher than the performance of other methods. Among them, mAP is 4.1% higher than the suboptimal method, and rank-1, rank-5, and rank-10 are 3.3%, 1.8%, and 1.8% higher than the suboptimal method, respectively. This result demonstrates that our method outperforms other methods for multi-resolution person ReID.

Appendix C.2 Experiments on Cross-resolution Datasets

Our method has been shown to be effective for person ReID when the images have multiple resolutions. To show that our technique can be used for general cross-resolution person ReID, our technique was validated using the simulated cross-resolution datasets MLR-DukeMTMC [1,13], MLR-CUHK03 [1,14], and MLR-Market1501 [1,15]. Table C2 presents the results of the cross-resolution person ReID method and our pyramid-resolution person restoration method on the simulated cross-resolution datasets.It can be observed that our proposed method outperforms existing approaches on these simulated cross-resolution datasets.

Appendix C.3 Ablation Study

We first investigate the constrained image restoration network loss of α, β. The average PSNR calculated from the restored images and the original images is used as the evaluation criterion. As shown in Table C3, we change only one of α, β at a time, and the

Table C3 Result on restoration loss with the changes of α, β.

$\alpha, (\beta = 1)$	0	0.2	0.5	1	2	5	10
PSNR	18.880	18.883	18.873	**18.883**	18.883	18.876	18.880
$\beta, (\alpha = 1)$	0	0.2	0.5	1	2	5	10
PSNR	18.880	18.870	18.880	**18.883**	18.876	18.880	18.880

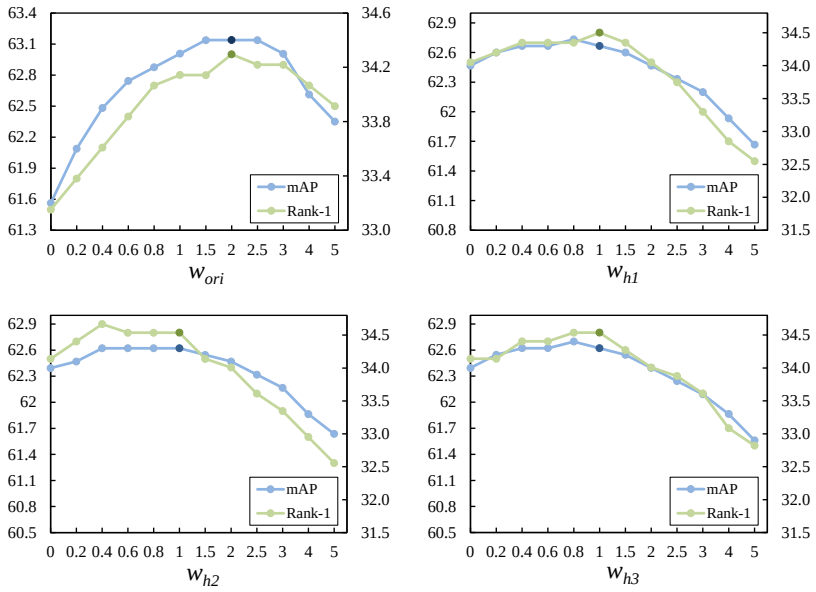

Figure C1 Results on feature distances with different weights. Only the weight of one feature distance is changed in each subfigure, and the weights of the remaining feature distances remain unchanged. Rank-1 corresponds to the left axis and mAP corresponds to the right axis.

Table C4 Ablation study (%) on MTA-ReID dataset. Ori refers to the feature distance calculated from the original dataset. HR1, HR2, HR3 and HR4 are the feature distances calculated from the four datasets obtained from the pyramid-resolution restoration network, respectively.

Feature Distance	mAP	Rank-1	Rank-5	Rank-10
Ori	30.8	59.7	74.1	78.2
HR1	30.1	58.9	73.4	77.8
HR2	29.9	58.6	73.2	77.4
HR3	30.1	58.3	73.1	77.6
HR4	29.8	58.6	73.3	77.6
Ori+HR1	33.7	62.2	75.6	79.4
Ori+HR2	33.6	62.0	75.4	79.3
Ori+HR3	33.7	61.9	75.4	79.5
Ori+HR4	33.7	62.1	75.4	79.6
Ori+HR1,2	34.5	62.9	75.8	79.7
Ori+HR1,2,3	**34.9**	**63.0**	**75.9**	**80.0**
Ori+HR1,2,3,4	34.8	**63.0**	**75.9**	79.9

other is fixed to 1. When we set β to 1, the best results are achieved whether we set α to 0.2, 1 or 2. When α is set to 1, β set to 1 gives the best results. Therefore, for ease of operation and simplicity of parameter setting, we recommend that both α and β be set to 1. This not only ensures the best results, but also facilitates practical operation and understanding.

Next we present the experimental result about the weights of feature distances during the fusion process on the MTA-ReID dataset. We change one weight value while fixing the others respectively. As shown in Figure C1, when we fixing the weights of w_{hj}, the value of w_{ori} is evaluated from 0 to 5, and when we set it to 2 both the mAP and rank-1 are the highest. Similarly, we also search for the best value of w_{h1}, w_{h2}, and w_{h3} respectively. In order to simplify the setting of the weights, we choose w_{ori} to be 2 and the other w_{hj} to be 1, which could achieve satisfying performance.

We further provide the ablation study of using different numbers of branches in our pyramid-resolution restoration framework, as shown in Table C4. Ori represents using only the original input images, which are not processed by our method. HR1, HR2, HR3 and HR4 represent using each of four branches respectively. It can be seen that without our pyramid-resolution restoration framework, merely using original images could only achieve rank-1 accuracy of 59.7%. When using single branch in the pyramid framework, the accuracies of HR1, HR2, HR3, and HR4 are lower than using original images, which is because the original dataset contains various resolutions of images to help enhance the performance. When using two branches, the rank-1 accuracy increases to around 62%. When three branches are all taken into consideration, the rank-1 accuracy achieves the best score of 63%. We further add another branch here, and it can be seen that using four branches could achieve competitive performance to three branches. However, as discussed in Appendix C.4, the computation complexity will increase when more branches are used.

In order to evaluate the effectiveness of our pyramid-resolution restoration network, we provide the experimental comparison, as shown in Table C5, by replacing the restoration network with simple bicubic interpolation here. Since bicubic interpolation operation can also be regarded as one kind of image restoration and enhancement technique, using the simple bicubic interpolation in our framework can also achieve rank-1 accuracy of 92.8% on MLR-Market1501. However, our deep learning based pyramid-

Figure C2 The visual effects of original images and pyramid-resolution images. Ori denotes the images in the original dataset, while HR1, HR2, and HR3 represent the pyramid-resolution images recovered by the pyramid-resolution restoration network. The HAN and the SwinIR represent the feature extractors used for generating the pyramid-resolution images.

Table C5 Evaluation result (%) of replacing the pyramid-resolution restoration network with simple bicubic interpolation on MLR-Market1501 dataset

Method	mAP	Rank-1	Rank-5	Rank-10
Ours (bicubic)	83.7	92.8	97.1	98.0
Ours (SwinIR)	84.3	93.7	97.3	98.4
Ours (HAN)	84.8	93.8	97.4	98.5

resolution image restoration network can generate restored person images with better quality and fidelity. Thus, our method could achieve rank-1 accuracy of 93.7% and 93.8% with two different restoration models, which demonstrates the effectiveness of our proposed pyramid-resolution person restoration for cross-resolution person ReID.

Finally, we investigate the visual effects of original images and pyramid-resolution images and the effect of different feature distances on the final ReID results in the feature fusion distance stage. As shown in Figure C2, the image restored by the HAN feature extractor is relatively smooth, while the image restored by the SwinIR feature extractor is relatively sharp. This may be due to the different focus of the two feature extractors on certain image features, but both restored images have a complementary effect to the original image. In addition, there is no significant visual difference when the pyramid-resolution images HR1, HR2, and HR3 are interpolated to the same size using bicubic interpolation. This is because when different high-resolution images are scaled down to the same low-resolution image, the visual difference is small, but the low-level data of the images has changed.

Appendix C.4 Model Complexity

We compare the model parameters of the proposed pyramid-resolution person restoration method with existing publicly available cross-resolution person ReID methods. As shown in Table C6, the number of parameters of our method, whether using the SwinIR-based feature extractor or the HAN-based feature extractor, is much less than that of existing open-code methods. The model parameters of the CSR-GAN method are three times of our method, and the model parameters of the PS-HRNet method are twice as high as our method. This proves that our method is simpler than some existing methods.

Considering that the feature fusion module will increase the testing time of person ReID, we further calculate the running time for different methods during testing on the MTA-ReID dataset, as shown in Table C7. The evaluation is conducted in Ubuntu system, with 64GB of memory, an Intel Core i9-10900K CPU, and a 24GB NVIDIA RTX 3090 GPU. We measure the running time on the MTA-ReID dataset, with 15,165 query images and 60,448 gallery images. Because our method utilizes multiple branches while OSNet [21] only uses single feature, the running time of OSNet is shorter than our method. However, our method still takes less running time than the baseline [18] and AGW [19]. Considering that our method could achieve superior performance than existing methods, the running time of our method is still comparable to other methods.

References

1 Jiao J, Zheng W S, Wu A, et al. Deep low-resolution person re-identification. In: Proceedings of the AAAI Conference on Artificial Intelligence. 2018, 32: 1
2 Li X, Zheng W S, Wang X, et al. Multi-scale learning for low-resolution person re-identification. In: Proceedings of the IEEE International Conference on Computer Vision, 2015. 3765–3773

Table C6 Number of model parameters for different methods.

Method	Params
CSR-GAN [3]	76.57M
PS-HRNet [11]	43.39M
Ours(SwinIR)	21.30M
Ours(HAN)	25.43M

Table C7 The running time for different methods during testing on the MTA-ReID dataset

Method	Time (s)
Strong Baseline [18]	1352.826
AGW [19]	1398.139
ABD [20]	392.137
OSNet [21]	122.014
Ours	770.132

3 Wang Z, Ye M, Yang F, et al. Cascaded SR-GAN for scale-adaptive low resolution person re-identification. In: Proceedings of the 27th International Joint Conference on Artificial Intelligence, 2018. 3891–3897
4 Li Y J, Chen Y C, Lin Y Y, et al. Recover and identify: a generative dual model for cross-resolution person re-identification. In: Proceedings of the IEEE International Conference on Computer Vision, 2019. 8090–8099
5 Munir A, Lyu C, Goossens B, et al. Resolution based feature distillation for cross resolution person re-identification. In: Proceedings of the IEEE International Conference on Computer Vision, 2021. 281–289
6 Zheng W S, Hong J, Jiao J, et al. Joint bilateral-resolution identity modeling for cross-resolution person re-identification. Int J Comput Vis, 2022, 1–21
7 Han K, Huang Y, Song C, et al. Adaptive super-resolution for person re-identification with low-resolution images. Pattern Recogn, 2021, 114: 107682
8 Jing X Y, Zhu X, Wu F, et al. Super-resolution person re-identification with semi-coupled low-rank discriminant dictionary learning. In: Proceedings of the IEEE Conference on Computer Vision and Pattern Recognition, 2015. 695–704
9 Mao S, Zhang S, Yang M. Resolution-invariant person re-identification. In: Proceedings of the 28th International Joint Conference on Artificial Intelligence, 2019. 883–889
10 Cheng Z, Dong Q, Gong S, et al. Inter-task association critic for cross-resolution person re-identification. In: Proceedings of the IEEE Conference on Computer Vision and Pattern Recognition, 2020. 2605–2615
11 Zhang G, Ge Y, Dong Z, et al. Deep high-resolution representation learning for cross-resolution person re-identification. IEEE Trans Image Process, 2021, 30: 8913–8925
12 Kohl P, Specker A, Schumann A, et al. The mta dataset for multi-target multi-camera pedestrian tracking by weighted distance aggregation. In: Proceedings of the IEEE Conference on Computer Vision and Pattern Recognition Workshops, 2020. 1042–1043
13 Zheng Z, Zheng L, Yang Y. Unlabeled samples generated by gan improve the person re-identification baseline in vitro. In: Proceedings of the IEEE International Conference on Computer Vision, 2017. 3754–3762
14 Zheng L, Shen L, Tian L, et al. Scalable person re-identification: a benchmark. In: Proceedings of the IEEE International Conference on Computer Vision, 2015. 1116–1124
15 Li W, Zhao R, Xiao T, et al. Deepreid: Deep filter pairing neural network for person re-identification. In: Proceedings of the IEEE conference on Computer Vision and Pattern Recognition, 2014. 152–159
16 Liang J, Cao J, Sun G, et al. Swinir: image restoration using swin transformer. In: Proceedings of the IEEE International Conference on Computer Vision, 2021. 1833–1844
17 Shi W, Caballero J, Huszar F, et al. Real-time single image and video super-resolution using an efficient sub-pixel convolutional neural network. In: Proceedings of the IEEE conference on Computer Vision and Pattern Recognition, 2016. 1874–1883
18 Luo H, Gu Y, Liao X, et al. Bag of tricks and a strong baseline for deep person re-identification. In: Proceedings of the IEEE Conference on Computer Vision and Pattern Recognition Workshops, 2019
19 Ye M, Shen J, Lin G, et al. Deep learning for person re-identification: a survey and outlook. IEEE Trans Pattern Anal Mach Intell, 2021, 44: 2872–2893
20 Chen T, Ding S, Xie J, et al. Abd-net: attentive but diverse person re-identification. In: Proceedings of the IEEE International Conference on Computer Vision, 2019. 8351–8361
21 Zhou K, Yang Y, Cavallaro A, et al. Learning generalisable omni-Scale Representations for person re-identification. IEEE Trans Pattern Anal Mach Intell, 2021
22 Wang Z, Hu R, Yu Y, et al. Scale-adaptive low-resolution person re-identification via learning a discriminating surface. In: Proceedings of International Joint Conference on Artificial Intelligence, 2016
23 Wu L, Liu L, Wang Y, et al. Learning resolution-adaptive representations for cross-resolution person re-identification. arXiv preprint arXiv:2207.13037, 2022
24 Zhang L, Xu Y, Zhao L, et al. Resolution independent person re-identification network. IET Computer Vision, 2022
25 Wu Z, Yu X, Zhu D, et al. SR-DSFF and FENet-ReID: A two-stage approach for cross resolution person re-identification. Comput Intell Neurosci, 2022
26 Rui S, Zi Y, Zhenghui Z, et al. Dual-stream coupling network with wavelet transform for cross-resolution person re-identification. Journal of Systems Engineering and Electronics, 2023
27 Li Y J, Chen Y C, Lin Y Y, et al. Cross-resolution adversarial dual network for person re-identification and beyond. arXiv preprint arXiv:2002.09274, 2020
28 Han K, Huang Y, Chen Z, et al. Prediction and recovery for adaptive low-resolution person re-identification. In: Proceedings of the European Conference on Computer Vision, 2020. 193–209
29 Chen Y C, Li Y J, Du X, et al. Learning resolution-invariant deep representations for person re-identification. In: Proceedings of the AAAI conference on artificial intelligence, 2019. 8215–8222
30 Zhang G, Chen Y, Lin W, et al. Low resolution information also matters: learning multi-resolution representations for person re-identification. arXiv preprint arXiv:2105.12684, 2021
31 He L, Wang Y, Liu W, et al. Foreground-aware pyramid reconstruction for alignment-free occluded person re-identification. In Proceedings of the IEEE/CVF international conference on computer vision. 2019: 8450-8459.
32 Chen G, Gu T, Lu J, et al. Person re-identification via attention pyramid. IEEE Transactions on Image Processing, 2021, 30: 7663-7676.
33 Zhang S, Yin Z, Wu X, et al. FPB: feature pyramid branch for person re-identification. arXiv preprint arXiv:2108.01901, 2021.